JOURNAL OF COMPUTATIONAL PHYSICS 8, 343–368 (1971)

A Discrete-variable Approach for Elastic-Plastic Wave Motions in Layered Solids

AHMED H. SAMEH

Center for Advanced Computation, University of Illinois, Urbana, Illinois 61801

Received February 2, 1971

A numerical technique is developed for the study of stress wave propagation in axisymmetric layered elastic-plastic solids. Although the theory of wave propagation in layered media is well established, analytic solutions of significant problems are possible only for linearly elastic cases. The underlying continuum is discretized into a finite number of discrete points consisting of mass points, at which displacements, velocities, and accelerations are defined, and stress points, at which the stress and strain tensors are defined. The equations of motion and the strain-displacement relations can be derived directly from this model and can be shown to be central finite difference analogs of the corresponding continuum equations. A noniterative scheme is used to integrate the equations of motion of the model numerically. The stability of this numerical scheme is investigated in detail. Convergence of the numerical scheme is also demonstrated by comparing solutions obtained by decreasing mesh sizes.

1. INTRODUCTION

A brief review of the literature [1, 2, 3, 4, 5] readily reveals that the analysis of wave motions in layered solid media in two or three dimensions presents some analytic difficulties. These difficulties are magnified if the material behavior is nonlinear or inelastic. In particular, any analytic solution of elastic-plastic wave motions is faced with having to consider the following:

(1) Moving elastic-plastic boundaries whose positions at a given time are not known beforehand.

(2) Unloading waves that may be generated, giving rise to a moving interface between the unloading and plastic regions of the material.

In consideration of the above difficulties, numerical methods of analysis are often the only feasible way to obtain solutions in a form that can be used for engineering purposes. Even then, approximations and idealizations of the real problem are invariably necessary. Some important numerical methods for determining wave motions include those of Alterman and Karal [6], Maenchen and

Sack [7], and Wilkins [8]. Ang and Rainer [9] developed a lumped-parameter model for studying stress-wave propagation in homogeneous axisymmetric solids, however the stability of their numerical scheme was not investigated. In this study, essentially the same lumped-parameter model is used for determining wave motions in axisymmetric elastic-perfectly-plastic layered solids, and the stability of the numerical method is investigated in detail.

It will be clear from the text that the resulting code is limited to those solids in which Hooke's law governs the stress-strain relations in the elastic range, initiation of yielding indicated by the vanishing of an invariant of the stress deviation (von Mises yield criterion is used), and the Prandtl–Reuss stress-strain rates relationships hold in the plastic range.

Two examples of practical significance are investigated:

(i) wave motions in a layered elastic-plastic solid induced by surface blast loading;

(ii) stresses and displacements in the same layered solid induced by sinusoidal loading.

2. The Mathematical Model

A mathematically consistent lumped parameter model is used in this study. The basic lumped parameter model of an axially symmetric solid can be described symbolically as shown in Fig. 1.

The underlying discrete model can be developed by properly concentrating the masses of volumental elements of the continuum at appropriate mass points, and defining average strains and stresses for volumental elements at appropriate stress points. Displacements, velocities, and accelerations are defined for such a model at the mass points, while strain tensors and stress tensors are defined at the stress points. Effectively, that material in the volumental element corresponding to a stress point is in homogeneous states of stress and strain.

Basic Relations for Small Displacements

The components of the strain tensor at an interior stress point, point "c" in Fig. 1, can be derived from simple geometrical arguments, as follows:

$$\epsilon_r^c = (u_2 - u_1)/\Delta r, \qquad \epsilon_\theta^c = u_5/r_5\,, \qquad \epsilon_z^c = (w_4 - w_3)/\Delta z,$$
$$\gamma_{rz}^c = (w_2 - w_1)/\Delta r + (u_4 - u_3)/\Delta z, \qquad \gamma_{r\theta}^c = \gamma_{z\theta}^c = 0, \tag{1}$$

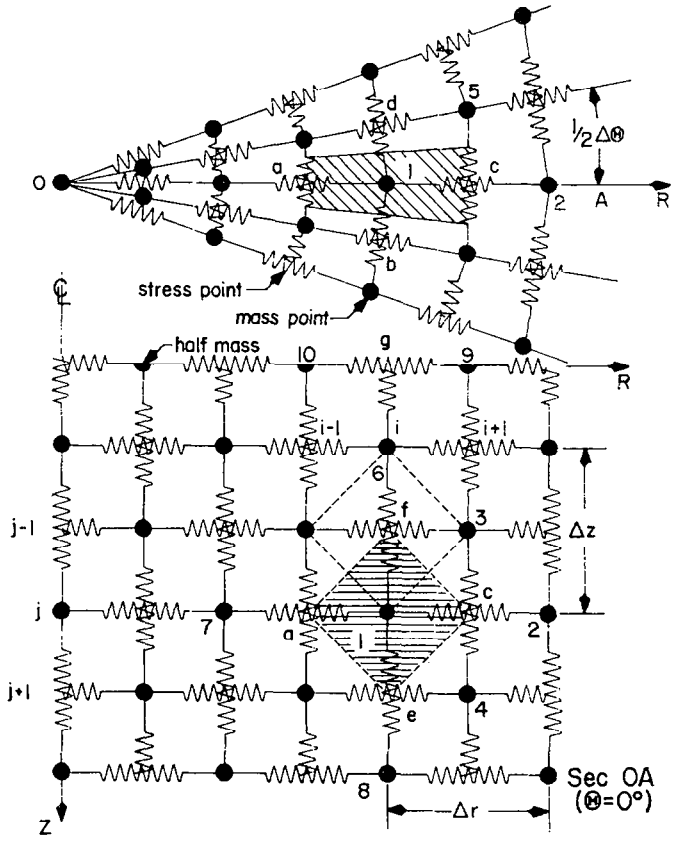

FIG. 1. Axisymmetric model in cylindrical coordinates.

where u and w denote the displacements in the radial and vertical directions, r_5 denotes the radius at point 5, and Δr and Δz are the mesh sizes in the radial and vertical directions, respectively. It is clear that the relations in (1) are central finite difference analogues (at point c) of the components of the strain tensor in the theory of small deformations [2],

$$\epsilon_r^c = \frac{\partial u}{\partial r}\bigg|_c, \qquad \epsilon_\theta^c = \frac{u}{r}\bigg|_c, \qquad \epsilon_z^c = \frac{\partial w}{\partial z}\bigg|_c,$$
$$\gamma_{rz}^c = \left(\frac{\partial u}{\partial z}\bigg|_c + \frac{\partial w}{\partial r}\bigg|_c\right), \qquad \gamma_{r\theta}^c = \gamma_{z\theta}^c = 0. \tag{2}$$

Equations of Motion

Figure 2 shows a volumental element of an interior mass point 1. Considering the dynamical equilibrium of this element in both the r and z directions, the equations of motion (in the absence of body forces) are

$$\frac{\sigma_r^{\,c} - \sigma_r^{\,a}}{\Delta r} + \frac{\tau_{rz}^{\,e} - \tau_{rz}^{\,f}}{\Delta z} + \frac{\sigma_r^{\,1} - \sigma_\theta^{\,1}}{r_1} = \zeta \ddot{u}$$

and (3)

$$\frac{\tau_{rz}^{\,c} - \tau_{rz}^{\,a}}{\Delta r} + \frac{\sigma_z^{\,e} - \sigma_z^{\,f}}{\Delta z} + \frac{\tau_{rz}^{\,1}}{r_1} = \zeta \ddot{w},$$

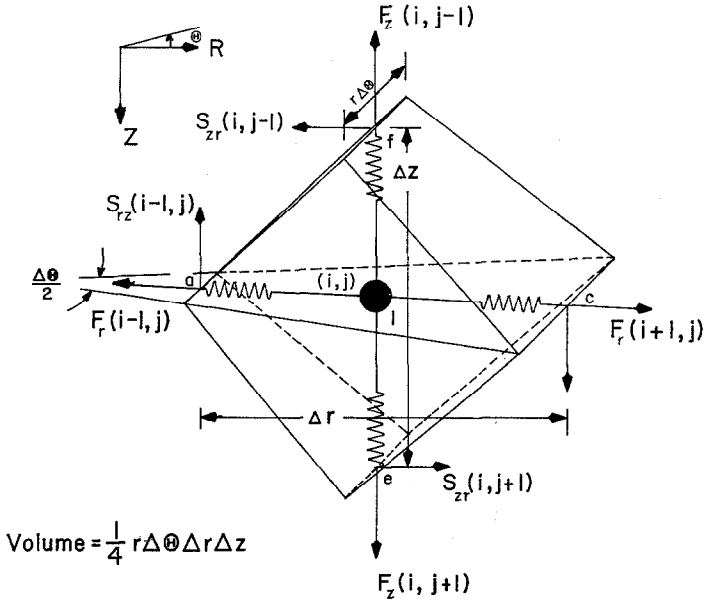

FIG. 2. A volumental element of an interior mass point.

where ζ is the mass density of the material at mass point 1, $\ddot{u}^1 = d^2u^1/dt^2$ and $\ddot{w}^1 = d^2w^1/dt^2$ are the accelerations in the r and z directions respectively, and $\sigma_r^{\,a}$, $\sigma_\theta^{\,a}$, $\sigma_z^{\,a}$, and $\tau_{rz}^{\,a}$ are the components of the stress tensor at stress point a. It should be observed that by virtue of symmetry, $\sigma_r^{\,1}$, $\sigma_\theta^{\,1}$, and $\tau_{rz}^{\,1}$ are actually equal to $\sigma_r^{\,d}$, $\sigma_\theta^{\,d}$, and $\tau_{rz}^{\,d}$ of stress point d or b. The terms in (3) are again the

central finite difference analogs (at point 1) of the corresponding terms of the differential equations of motion in cylindrical polar coordinates [2],

$$\frac{\partial \sigma_r}{\partial r} + \frac{\partial \tau_{rz}}{\partial z} + \frac{\sigma_r - \sigma_\theta}{r} = \zeta \ddot{u},$$
$$\frac{\partial \tau_{rz}}{\partial r} + \frac{\partial \sigma_z}{\partial z} + \frac{\tau_{rz}}{r} = \zeta \ddot{w}. \tag{4}$$

The significance of the above model may be observed as follows. The model is developed on the basis of defining certain average physical quantities of the continuum at a finite number of discrete points. On the average, therefore, the model can be expected to have the same properties as the idealized continuum.

Boundary Conditions

The two types of boundary conditions, namely, stress and displacement boundary conditions are readily defined for the model. This can be done by specifying the stresses and displacements at the corresponding stress and mass points that are on the boundary. In the process of the numerical solution, the stress boundary conditions are included in the equations of motion of the appropriate boundary mass points, while displacement boundary conditions are included in the strain displacement relations for the appropriate stress points.

3. Constitutive Relationships

In order to simplify the problem mathematically and still retain the basic property of irreversibility or inelasticity of a material, the present study assumes an elastic-perfectly plastic medium. The general constitutive relationships for an elastic-perfectly-plastic material are extensively available [10, 11, 12], and the constitutive equations for problems with axial symmetry can be obtained.

Stress Strain Relations in the Elastic Range

In the elastic range, Hooke's law may be expressed as follows:

$$\begin{bmatrix} \sigma_r \\ \theta_\theta \\ \sigma_z \\ \tau_{rz} \end{bmatrix} = \begin{bmatrix} (\lambda + 2\mu) & \lambda & \lambda & 0 \\ \lambda & (\lambda + 2\mu) & \lambda & 0 \\ \lambda & \lambda & (\lambda + 2\mu) & 0 \\ 0 & 0 & 0 & \mu \end{bmatrix} \begin{bmatrix} \epsilon_r \\ \epsilon_\theta \\ \epsilon_z \\ \gamma_{rz} \end{bmatrix}, \tag{5}$$

where λ and μ are Lame's constants,

$$\lambda = \nu E/(1 + \nu)(1 - 2\nu), \qquad \mu = E/2(1 + \nu), \tag{6}$$

in which ν is Poisson's ratio and E is Young's modulus.

Yield Criterion

The von Mises yield criterion is assumed to determine the initiation of yielding. In case of axial symmetry, von Mises condition is

$$J_2 = (1/6)[(\sigma_r - \sigma_\theta)^2 + (\sigma_r - \sigma_z)^2 + (\sigma_z - \sigma_\theta)^2] + \tau_{rz}^2 = k_0^2, \tag{7}$$

where k_0 is the yield limit in simple shear; $k_0 = \sigma_y/\sqrt{3}$, σ_y being the yield stress of the material in simple tension.

Stress-Strain Relations in the Plastic Range

When $J_2 = k_0^2$ and the rate of distortional work $\dot{W}$ is positive, the material undergoes irreversible plastic flow. The Prandtl–Reuss stress-strain law is assumed to describe the behavior of the material in the plastic range. For the axially symmetric case, the Prandtl–Reuss stress-strain rate relations take the following form [13]:

$$\{\dot{\sigma}\} = [P]\{\dot{\epsilon}\}, \tag{8}$$

where

$$\{\dot{\sigma}\} = \{\dot{\sigma}_r\,,\ \dot{\sigma}_\theta\,,\ \dot{\sigma}_z\,,\ \dot{\tau}_{rz}\};\ \{\dot{\epsilon}\} = \{\dot{\epsilon}_r\,,\ \dot{\epsilon}_\theta\,,\ \dot{\epsilon}_z\,,\ \dot{\gamma}_{rz}\} \tag{9}$$

and the matrix P is symmetric and its elements are defined by

$$\begin{aligned}
p_{ii} &= K_0 + K_1[1 - (\Sigma_i^2/12k_0^2)], \qquad i = 1, 2, 3,\\
p_{ij} &= K_0 - (K_1/2)[1 + (\Sigma_i\Sigma_j)/6k_0^2], \qquad i, j = 1, 2, 3, \quad i \neq j,\\
p_{44} &= (3K_1/4)[1 - (\tau_{rz}^2/k_0^2)],\\
p_{i4} &= -K_1\Sigma_i\tau_{rz}/4k_0^2, \qquad i = 1, 2, 3,
\end{aligned} \tag{10}$$

where

$$\begin{aligned}
&K_0 = E/3(1 - 2\nu), \qquad K_1 = 2E/3(1 + \nu),\\
&\Sigma_1 = (2\sigma_r - \sigma_\theta - \sigma_z), \qquad \Sigma_2 = (2\sigma_\theta - \sigma_r - \sigma_z), \quad \text{and}\\
&\Sigma_3 = (2\sigma_z - \sigma_r - \sigma_\theta).
\end{aligned} \tag{11}$$

The rate of distortional work is defined by,

$$\dot{W} = (1/3)[\dot{\epsilon}_r\Sigma_1 + \dot{\epsilon}_\theta\Sigma_2 + \dot{\epsilon}_z\Sigma_3] + \dot{\gamma}_{rz}\tau_{rz}\,. \tag{12}$$

Elastic Unloading and Reloading

Whenever $J_2 = k_0^2$ and $\dot{W} < 0$, the material is starting to unload from a plastic state. Unloading is assumed to be incrementally elastic, and since the instantaneous

stress and strain rates are proportional, the time-rate form of Hooke's law describes the behavior of the material during unloading and on any subsequent reloading (where $J_2 < k_0^2$, $\dot{W} > 0$). The rate form of Hooke's law is,

$$\{\dot{\sigma}\} = H\{\dot{\epsilon}\}, \tag{13}$$

where H is the coefficient matrix in (5).

4. Numerical Techniques

Numerical Integration of Equations of Motion

Assuming that at a generic time t, all physical quantities, consisting of accelerations, velocities, displacements, strains, stresses, and the appropriate material behavior at all stress and mass points are known, the corresponding quantities at the end of time $t + \Delta t$, where Δt is the chosen time increment, may be obtained by performing the following sequence of calculations:

(1) The sequence is started with initial trial accelerations $\ddot{u}^{t+\Delta t}$ and $\ddot{w}^{t+\Delta t}$ equal to those obtained using the known components of the stress tensor at time t in (3), that is, the accelerations at time t.

(2) Using the calculated accelerations, the velocities $\dot{u}^{t+\Delta t}$ and $\dot{w}^{t+\Delta t}$ are obtained using the following quadrature relations:

$$\begin{aligned}
\dot{u}^{t+\Delta t} &= \dot{u}^t + (\Delta t/2)(\ddot{u}^t + \ddot{u}^{t+\Delta t}),\\
\dot{w}^{t+\Delta t} &= \dot{w}^t + (\Delta t/2)(\ddot{w}^t + \ddot{w}^{t+\Delta t}),\\
u^{t+\Delta t} &= u^t + \Delta t\, \dot{u}^t + (\Delta t)^2(\ddot{u}^t/2),\\
w^{t+\Delta t} &= w^t + \Delta t\, \dot{w}^t + (\Delta t)^2(\ddot{w}^t/2).
\end{aligned} \tag{14}$$

(3) From the displacements and velocities computed in step 2, the strains are obtained by (1), and the strain rates at stress point c, Fig. 1, are defined by expressions similar to (1), where the displacements are replaced by the velocities $\dot{u}$ and $\dot{w}$.

(4) At the end of each time increment, the yield criterion given by (7) is examined at each stress point for initiation of yielding. If the stress point is still in the elastic range ($J_2 < k_0^2$), then the stresses are obtained using (5). A stress point is in the plastic region if $J_2 = k_0^2$ and $\dot{W} > 0$, the stress rates are then obtained from (8), and the total stresses are obtained by

$$\{\sigma\}^{t+\Delta t} = \{\sigma\}^t + \Delta t \cdot \{\dot{\sigma}\}^t. \tag{15}$$

If the condition of von Mises is violated, that is, $J_2 > k_0^2$, the stresses are adjusted in order to maintain the requirement of (7), [13]. The adjusted stresses are as follows:

$$\{\sigma\} = (1 - \xi)\{\sigma'\} + \xi s\{e'\}, \tag{16}$$

where $\{\sigma'\}$ is the unadjusted stress vector,

$$s = \tfrac{1}{3}(\sigma_r + \sigma_\theta + \sigma_z), \qquad \{e'\} = \{1, 1, 1, 0\}, \qquad \xi = (J_2 - k_0^2)/2k_0^2 \tag{17}$$

in which $(J_2 - k_0^2)$ represents the deviation from the yield surface. Finally, a stress point is in the unloading region if $J_2 - k_0^2 = 0$ and $\dot{W} < 0$, the stress rates are determined from the rate form of Hooke's law (13), and the stresses are obtained using (15).

(5) Step 1 is repeated to find the new values of the accelerations and the procedure is repeated until the difference in the calculated values of $\ddot{u}$ and $\ddot{w}$ of the last two cycles is less than a given permissible error. If so, the time is incremented by Δt and steps 1 through 5 are repeated.

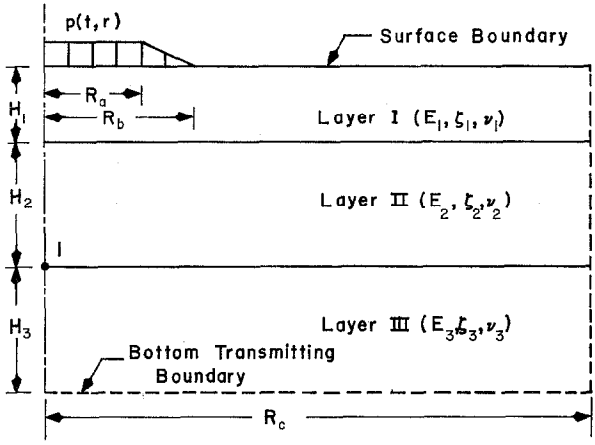

FIG. 3. Partially loaded layered half space.

Calculation of Stresses at Special Points

The stresses of stress points on the horizontal surface boundary of a half space, Fig. 3, on the axis of symmetry, or on an interface between two layers, require special treatment different from those described in the above section.

(a) *Surface Boundary.* For the horizontal surface in Fig. 3, the boundary conditions are:

$$\sigma_z = \begin{cases} p(t, r) & \cdots\ 0 \leqslant r < R_b\ ; \quad \tau_{rz} = 0; \\ 0 & \cdots\ \quad r \geqslant R_b\ . \end{cases} \tag{18}$$

The following strain components of stress point g, Fig. 1, can be obtained:

$$\epsilon_r^g = (u_9 - u_{10})/\Delta r; \qquad \epsilon_\theta^g = u_g/r_g; \qquad \gamma_{rz}^g = 0. \tag{19}$$

In the elastic range, the stresses may be obtained through (5); thus

$$\begin{aligned} \epsilon_z &= [\sigma_z - \lambda(\epsilon_r + \epsilon_\theta)]/(\lambda + 2\mu), \\ \sigma_r &= (\lambda + 2\mu)\,\epsilon_r + \lambda(\epsilon_\theta + \epsilon_z), \\ \sigma_\theta &= (\lambda + 2\mu)\,\epsilon_\theta + \lambda(\epsilon_r + \epsilon_z), \end{aligned} \tag{20}$$

whereas in the plastic range, (8) can be used to determine the unknown stress rates $\dot{\sigma}_r$ and $\dot{\sigma}_\theta$ as follows:

$$\begin{aligned} \dot{\epsilon}_z &= [\dot{\sigma}_z - (p_{13}\dot{\epsilon}_r + p_{23}\dot{\epsilon}_\theta)]/p_{33}, \\ \dot{\sigma}_r &= [p_{11}\dot{\epsilon}_r + p_{12}\dot{\epsilon}_\theta + p_{13}\dot{\epsilon}_z], \\ \dot{\sigma}_\theta &= [p_{12}\dot{\epsilon}_r + p_{22}\dot{\epsilon}_\theta + p_{23}\dot{\epsilon}_z], \end{aligned} \tag{21}$$

where p_{mn} are the coefficients of the matrix P in (8). The total stresses are then obtained by (15).

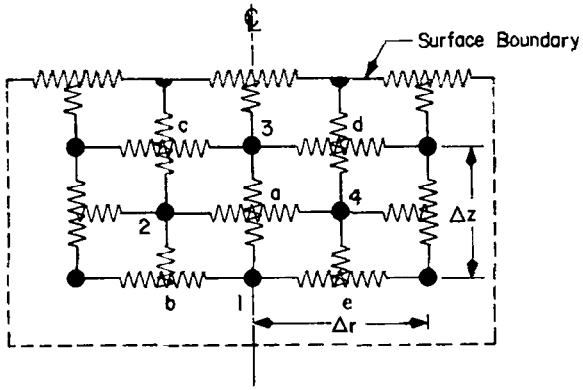

FIG. 4. Strain-displacement relations on the axis of symmetry.

(b) *Axis of Symmetry.* Strain-displacement relations for a point on the axis of symmetry such as point a, Fig. 4, are:

$$\epsilon_r^a = 2u_4/\Delta r; \qquad \epsilon_\theta^a = \epsilon_r^a; \qquad \epsilon_z^a = (w_1 - w_3)/\Delta z; \qquad \gamma_{rz}^a = 0. \tag{22}$$

Then calculation of the stresses in the elastic, plastic, and unloading ranges proceed as described for an intermediate stress point.

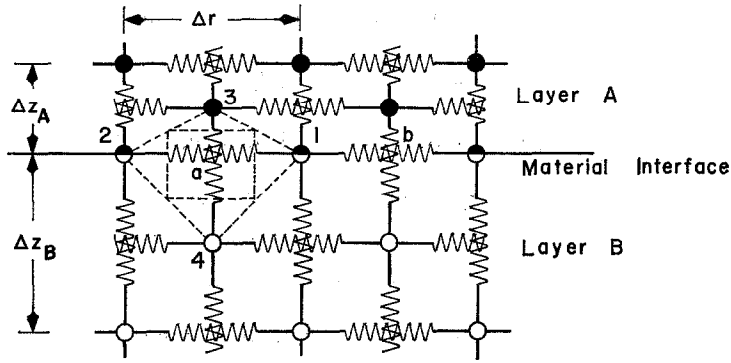

FIG. 5. Boundary conditions at an interface between two layers.

(c) *Interface between two layers.* Figure 5 shows an interface between two layers of material A and B. Assuming that the layers are in "welded contact" [2], the boundary conditions to be satisfied are

$$\begin{aligned} u_1{}^A &= u_1{}^B; \qquad w_1{}^A = w_1{}^B \\ (\sigma_z{}^a)^A &= (\sigma_z{}^a)^B; \qquad (\tau_{rz}^a)^A = (\tau_{rz}^a)^B. \end{aligned} \tag{23}$$

The radial and tangential strains at stress point a, Fig. 5, can be obtained directly.

$$\epsilon_r{}^a = (u_1 - u_2)/\Delta r; \qquad \epsilon_\theta{}^a = u_a/r_a\,. \tag{24}$$

In the elastic range the stresses σ_z in the two layers at the interface are expressed by (5). Equating $\sigma_z{}^A$ and $\sigma_z{}^B$, a relation between $\epsilon_z{}^A$ and $\epsilon_z{}^B$ is obtained:

$$\epsilon_z{}^A = [(\lambda_B + 2\mu_B)/(\lambda_A + 2\mu_A)]\,\epsilon_z{}^B + [(\lambda_B - \lambda_A)/(\lambda_A + 2\mu_A)](\epsilon_r + \epsilon_\theta). \tag{25}$$

Moreover, from Fig. 5, the total elongation at stress point a may be expressed as

$$w_4 - w_3 = (\Delta z_A \epsilon_z{}^A + \Delta z_B \epsilon_z{}^B)/2. \tag{26}$$

Solving (25) and (26) for $\epsilon_z{}^A$ and $\epsilon_z{}^B$,

$$\begin{aligned} \epsilon_z{}^A &= \chi_1 \epsilon_z + \chi_2(\epsilon_r + \epsilon_\theta), \\ \epsilon_z{}^B &= (1 + m^{-1})\,\epsilon_z - m^{-1}\epsilon_z{}^A, \end{aligned} \tag{27}$$

where

$$\begin{aligned} \epsilon_z &= 2(w_4 - w_3)/(\Delta z_A + \Delta z_B), \\ \chi_1 &= (1 + m)(\lambda_B + 2\mu_B)/[m(\lambda_A + 2\mu_A) + (\lambda_B + 2\mu_B)], \\ \chi_2 &= m(\lambda_B - \lambda_A)/[m(\lambda_A + 2\mu_A) + (\lambda_B + 2\mu_B)], \\ m &= \Delta z_B/\Delta z_A\,. \end{aligned} \tag{28}$$

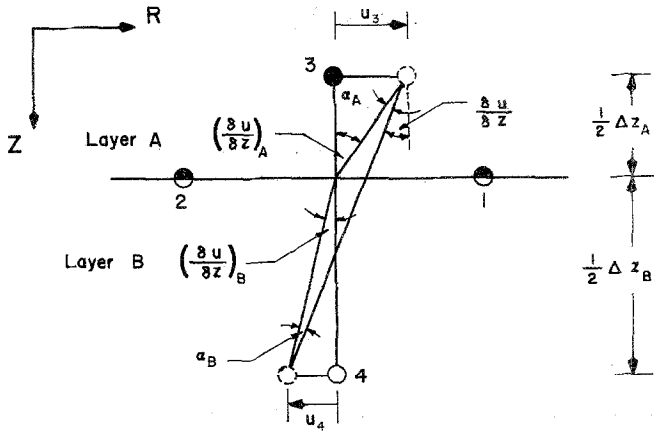

FIG. 6. Shear strain at a stress point on an interface.

Consequently, from (5), expressions for the diagonal components of the stress tensor at point a can be obtained. It may be observed that the radial and tangential stresses are discontinuous at an interface; however, for calculating the accelerations of the mass points at an interface, these stresses are averaged as follows:

$$\sigma_r = [\sigma_r^A + m\sigma_r^B]/(1 + m); \qquad \sigma_\theta = [\sigma_\theta^A + m\sigma_\theta^B]/(1 + m). \tag{29}$$

Equating the shear stresses in the two layers at the material interface yields

$$\underset{A}{\mu}\gamma_{rz}^A = \underset{B}{\mu}\gamma_{rz}^B, \tag{30}$$

where

$$\gamma_{rz}^A = \frac{\partial w}{\partial r} + \left(\frac{\partial u}{\partial z}\right)_A, \qquad \gamma_{rz}^B = \frac{\partial w}{\partial r} + \left(\frac{\partial u}{\partial z}\right)_B, \tag{31}$$

in which $(\partial u/\partial z)_A$ and $(\partial u/\partial z)_B$ are as defined in Fig. 6.

$$\left(\frac{\partial u}{\partial z}\right)_A = \left(\frac{\partial u}{\partial z}\right) + \alpha_A; \qquad \left(\frac{\partial u}{\partial z}\right)_B = \left(\frac{\partial u}{\partial z}\right) - \alpha_B. \tag{32}$$

Combining (31) and (32),

$$\gamma_{rz}^A = \gamma_{rz} + \alpha_A, \qquad \gamma_{rz}^B = \gamma_{rz} - \alpha_B, \tag{33}$$

where $\gamma_{rz} = \partial u/\partial z + \partial w/\partial r$, or, from Fig. 6,

$$\gamma_{rz} = [2(u_4 - u_3)/(\Delta z_A + \Delta z_B)] + [(w_1 - w_2)/\Delta r]. \tag{34}$$

Observing that for small displacements, $\Delta z_A \cdot \alpha_A = \Delta z_B \cdot \alpha_B$, that is, $\alpha_A = m\alpha_B$, then (30) and (33) yield

$$\tau_{rz} = [(1 + m)\,\mu_A\mu_B/(m\mu_A + \mu_B)]\,\gamma_{rz}\,. \tag{35}$$

In the plastic range, the stress-strain rates relationship is expressed by (8). At an interface $\dot{\sigma}_z{}^A = \dot{\sigma}_z{}^B$; thus, using this condition with (8), (27), (33), and (34), the following equation for $\dot{\alpha}_A$ and $\dot{\epsilon}_z{}^A$ is obtained:

$$D_1\dot{\epsilon}_z{}^A + D_2\dot{\alpha}_A = D_3\,, \tag{36}$$

where

$$\begin{gathered} D_1 = p_{33}^A + m^{-1}p_{33}^B\,, \qquad D_2 = p_{34}^A + m^{-1}p_{34}^B\,, \\ D_3 = (p_{13}^B - p_{13}^A)\,\dot{\epsilon}_r + (p_{23}^B - p_{23}^A)\,\dot{\epsilon}_\theta + (1 + m^{-1})\,p_{33}^B\dot{\epsilon}_z + (p_{34}^B - p_{34}^A)\,\dot{\gamma}_{rz}\,, \end{gathered} \tag{37}$$

and $\dot{\epsilon}_r$, $\dot{\epsilon}_\theta$, $\dot{\epsilon}_z$ and $\dot{\gamma}_{rz}$ are given by the rate form of (24), (28), and (34). Considering next the shear stress rate at the interface, $\dot{\tau}_{rz}^A = \dot{\tau}_{rz}^B$; then, using (8), the rate form of (27), and (34), a second equation in $\dot{\alpha}_A$ and $\dot{\epsilon}_z{}^A$ is obtained:

$$D_4\dot{\epsilon}_z{}^A + D_5\dot{\alpha}_A = D_6\,, \tag{38}$$

where

$$\begin{gathered} D_4 = D_2\,, \qquad D_5 = p_{44}^A + m^{-1}p_{44}^B\,, \\ D_6 = (p_{14}^B - p_{14}^A)\,\dot{\epsilon}_r + (p_{24}^B - p_{24}^A)\,\dot{\epsilon}_\theta + (1 + m^{-1})\,p_{34}^A\dot{\epsilon}_z + (p_{44}^B - p_{44}^A)\,\dot{\gamma}_{rz}\,. \end{gathered} \tag{39}$$

From (36) and (38),

$$\begin{aligned} \dot{\epsilon}_z{}^A &= (D_3D_5 - D_2D_6)/(D_1D_5 - D_2D_4), \\ \dot{\alpha}_A &= (D_1D_6 - D_3D_4)/(D_1D_5 - D_2D_4). \end{aligned} \tag{40}$$

Consequently, all the strain rates are defined, using (8) the stress rates can be determined, and the total stresses are obtained by (15). Again, the radial and tangential stress rates are averaged, as in (29), for the purpose of calculating the accelerations at the interface mass points.

Since unloading is assumed to follow the rate form of Hooke's law, the stress rates at the interface can be obtained directly as the time derivative of the corresponding stresses derived for the elastic range.

5. Convergence and Stability of the Numerical Scheme

This section is concerned with the conditions that must be satisfied in order to assure that the solution of the equations of motion, which are central finite

difference equations, is a reasonably accurate and valid approximation to the solution of the corresponding system of hyperbolic partial differential equations. Such conditions have been established for some linear hyperbolic systems of difference equations [14, 15, 16, 17, 18].

The method developed by von Neumann [19] and discussed in detail by O'Brien, Hyman and Kaplan [20] is followed in the analysis of the stability of the numerical scheme used herein. Essentially, the method expresses the errors of a solution in terms of a finite Fourier series. The behavior of the error is then examined as time increases such that at $t = 0$, the errors reduce to the given series.

Denoting the errors at the mesh points along $t = 0$ and the domain $0 \leqslant r \leqslant N\Delta r$, and, $0 \leqslant z \leqslant M\Delta z$ by $E(p\Delta r, q\Delta z)$ or $E_{p,q}$, where $p = (i - 1)/2$, for $i = 1, 2,..., 2N + 1$, and $q = (j - 1)/2$, for $j = 1, 2,..., 2M + 1$; it is possible to express the error in the displacement components as follows:

$$E_{p,q} = \sum_{n=0}^{N} \sum_{m=0}^{M} A_{mn} \exp[I\alpha_n p\,\Delta r + I\beta_m q\,\Delta z] \tag{41}$$

in which $I = \sqrt{-1}$, A_{mn} are constant coefficients, α and β are frequencies that can be chosen arbitrarily. Since the system of equations under consideration (equations of motion), are linear difference equations, superposition applies; hence, only one term of (41) needs to be considered. The coefficients A_{mn}, being constants, can be neglected. Therefore, for $t = v\Delta t > 0$,

$$\begin{aligned} E_{p,q,v} &= \exp[I(\alpha p\Delta r + \beta q\Delta z) + \gamma t] \\ &= \eta^v \cdot \exp[I(\alpha p\Delta r + \beta q\Delta z)], \end{aligned} \tag{42}$$

where $\eta = \exp(\gamma\Delta t)$.

Equation (42) shows clearly that the error $E_{p,q,v}$ will not increase with time if $|\eta| \leqslant 1$.

The equations of motion derived using the model in terms of the displacement components u and w can be obtained from (3). Denoting the coordinates of point 1 by (i, j), the first of (3) yields

$$\begin{aligned} \zeta\ddot{u}^t = {} & [(\lambda + 2\mu)/\Delta r^2][u(i-2, j, k) - 2u(i, j, k) + u(i+2, j, k)] \\ & + [(\lambda + 2\mu)/p\Delta r^2][u(i+1, j, k) - u(i-1, j, k)] \\ & - [(\lambda + 2\mu)/p^2\Delta r^2][u(i, j, k)] \\ & + (\mu/\Delta z^2)[u(i, j-2, k) - 2u(i, j, k) + u(i, j+2, k)] \\ & + [(\lambda + \mu)/\Delta r\Delta z][w(i+1, j+1, k) - w(i-1, j+1, k) \\ & - w(i+1, j-1, k) + w(i-1, j-1, k)]. \end{aligned} \tag{43}$$

From (14) the following expressions may be obtained:

$$\dot{u}^t = \dot{u}^{t-\Delta t} + (\Delta t/2)(\ddot{u}^t + \ddot{u}^{t-\Delta t}),$$
$$u^t = u^{t-\Delta t} + \Delta t \dot{u}^{t-\Delta t} + (\Delta t)^2(\ddot{u}^{t-\Delta t}/2),$$

and

$$u^{t+\Delta t} = u^t + \Delta t \dot{u}^t + (\Delta t)^2(\ddot{u}^t/2).$$

Subtracting the second equation from the third and using the first, the following equation for $u^{t+\Delta t}$ is obtained:

$$u^{t+\Delta t} = 2u^t - u^{t-\Delta t} + (\Delta t)^2 \ddot{u}^t.$$

Similarly,

$$w^{t+\Delta t} = 2w^t - w^{t-\Delta t} + (\Delta t)^2 \ddot{w}^t. \tag{44}$$

From the first of (44), the left side of (43) becomes,

$$[u(i, j, k+1) - 2u(i, j, k) + u(i, j, k-1)]\, \zeta/(\Delta t)^2. \tag{45}$$

Assuming that each term in (43) contains errors of the form of (42), it can be shown that the error function $E_{p,q,v}$ also satisfies a difference equation of the form of (43). Thus, replacing each $u(i + \delta_1, j + \delta_2, k + \delta_3)$ or $w(i + \delta_1, j + \delta_2, k + \delta_3)$ in (43) by

$$E_{p+\frac{\delta_1}{2}, q+\frac{\delta_2}{2}, v+\delta_3} = n^{v+\delta_3} \cdot \exp[I\alpha(p + 1/2\delta_1)\,\Delta r + I\beta(q + 1/2\delta_2)\,\Delta z] \tag{46}$$

(where each of δ_1, δ_2, or δ_3 may be the integers 0, ± 1), one obtains

$$\frac{\zeta}{(\Delta t)^2} \cdot \frac{(1-\eta)^2}{\eta} = \left[-4\left(\frac{\lambda + 2\mu}{\Delta r^2}\right)\left(\sin\frac{\alpha\,\Delta r}{2}\right)^2 - \frac{4\mu}{\Delta z^2}\left(\sin\frac{\beta\,\Delta z}{2}\right)^2 - \frac{\lambda + 2\mu}{p^2\,\Delta r^2} - 4\left(\frac{\lambda+\mu}{\Delta r\,\Delta z}\right)\sin\frac{\alpha\,\Delta r}{2}\sin\frac{\beta\,\Delta z}{2}\right] + I\left[\frac{2(\lambda - 2\mu)}{p\,\Delta r^2}\sin\frac{\alpha\,\Delta r}{2}\right]. \tag{47}$$

By the same token the second of Eq. (3) yields

$$\frac{\zeta}{(\Delta t)^2} \cdot \frac{(1-\eta)^2}{\eta} = \left[-4\left(\frac{\lambda + 2\mu}{\Delta z^2}\right)\left(\sin\frac{\beta\,\Delta z}{2}\right)^2 - \frac{4\mu}{\Delta r^2}\left(\sin\frac{\alpha\,\Delta r}{2}\right)^2 - 4\left(\frac{\lambda+\mu}{\Delta r\,\Delta z}\right)\sin\frac{\alpha\,\Delta r}{2}\sin\frac{\beta\,\Delta z}{2}\right] + I\left[\frac{2\mu}{p\,\Delta r^2}\sin\frac{\alpha\,\Delta r}{2} + 2\left(\frac{\lambda+\mu}{p\,\Delta r\,\Delta z}\right)\sin\frac{\beta\,\Delta z}{2}\right]. \tag{48}$$

Equating the real and imaginary parts of the right sides of (47) and (48), one gets

$$(\sin \alpha \Delta r/2)^2 = (\Delta r/\Delta z)^2(\sin \beta \Delta z/2)^2 = (1 - \nu)/2p^2 \tag{49}$$

and

$$\sin(\alpha \Delta r/2) = (\Delta r/\Delta z) \sin(\beta \Delta z/2). \tag{50}$$

Substituting either of (49) or (50) in (47) or (48) yields an equation of the form:

$$\eta^2 - 2\eta B + 1 = 0. \tag{51}$$

Therefore,

$$\eta = B \pm (B^2 - 1)^{1/2}. \tag{52}$$

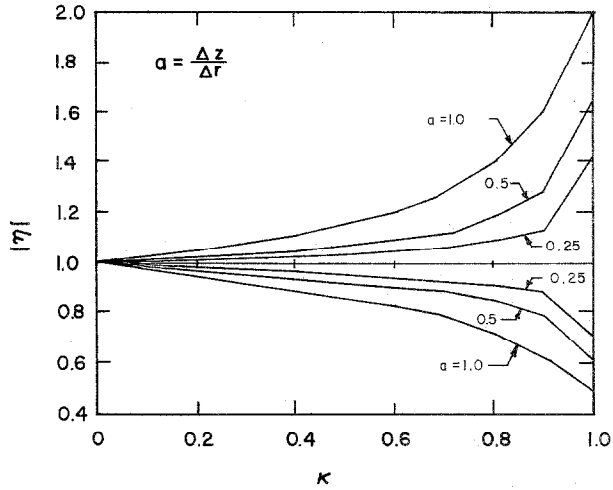

FIG. 7. Modulus of η vs. κ for $p = 1.0$.

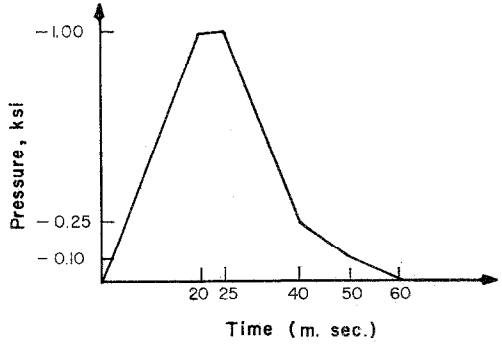

FIG. 8. Directly induced blast pressure pulse.

The largest absolute value of η is obtained if B is of maximum modulus. It can be shown that substituting (50) in (48) yields the maximum modulus of B; specifically, in this case,

$$B = (1 - 2\kappa^2 \sin^2(\beta \Delta z/2)) + I(a\kappa^2 \sin(\beta \Delta z/2))/2p, \tag{53}$$

where

$$\kappa^2 = 2(\Delta t/\Delta z)^2 c_d^2 \qquad \text{and} \qquad a = (\Delta z/\Delta r) \leqslant 1, \tag{54}$$

c_d being the dilatational wave speed. For large radii, that is, as $p \to \infty$, it can be shown that $|\eta| \leqslant 1.0$, that is, the difference scheme is stable for

$$\Delta t \leqslant \Delta z/\sqrt{2}\, c_d\,, \tag{55}$$

which is also the stability criterion of plane wave motion [13].

The absolute value of η was evaluated numerically from (52) and (53) for $p = 1.0$ and for different values of κ and a. Figure 7 shows that one of the roots of (52) is greater than 1, indicating local instability in the neighborhood of the axis of symmetry. An approximate stability condition may be obtained by observing that, from Fig. 7 for $\kappa \leqslant 0.5$ and $a \leqslant 0.5$ ($a = 1.0$ being the worst case), $|\eta|$ is not much larger than 1. Thus, an appropriate condition may be stated as

$$\Delta t \leqslant \Delta z/3c_d\,. \tag{56}$$

An elastic homogeneous half space is used for the purpose of studying the effect of mesh sizes on the behavior of the numerical solutions. The right side of the

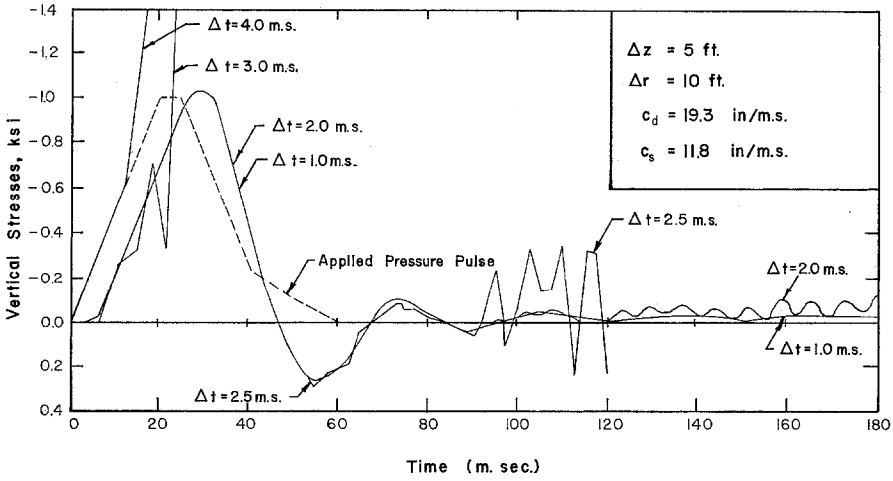

FIG. 9. History of vertical stresses at $Z = 10$ ft (axis of symmetry).

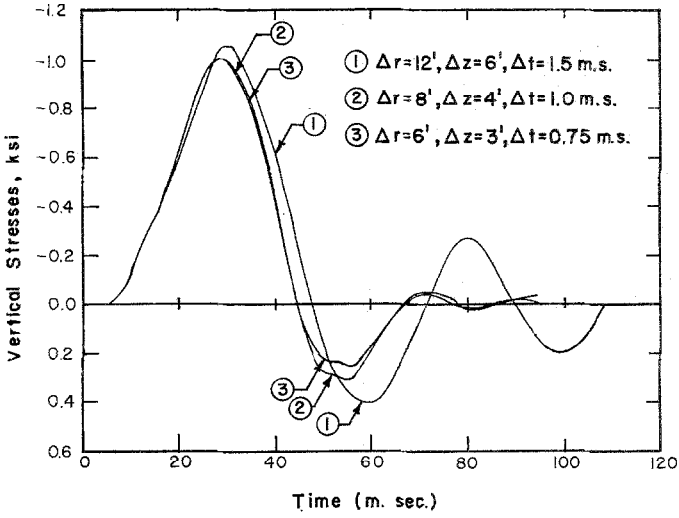

FIG. 10. History of vertical stresses, $R = 0$, $Z = 12$ ft.

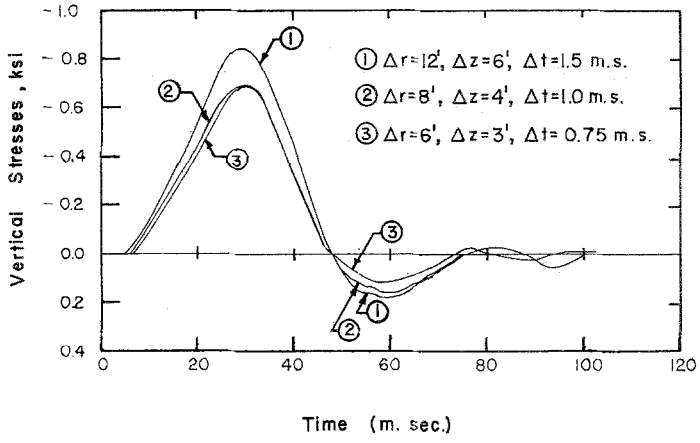

FIG. 11. History of vertical stresses, $R = 12$, $Z = 12$ ft.

half space is assumed to be confined laterally while the bottom edge is provided with a transmitting boundary, Ang (private communication). Figure 3 shows the half space, and the pressure pulse is shown in Fig. 8. The material constants are chosen to be:

$$E_1 = E_2 = E_3 = 75 \text{ ksi}, \qquad \zeta = 150 \text{ lb/ft}^3, \qquad \nu = 0.2,$$
$$c_d = 1600 \text{ fps}, \qquad c_s = 980 \text{ fps},$$

c_s being the shear wave speed. The results are shown in Figs. 9–11. Figure 9

shows the history of vertical stresses at a point on the axis of symmetry; the solution is unstable for $\Delta t = 4.0$, 3.0, and 2.5 msec, while $\Delta t = 1.0$ msec does not show instability for reasonable calculation times. The practical stability condition given by (56) requires $\Delta t = 1.10$ msec. Figures 10 and 11 provide an indication of the convergence of the solutions corresponding to decreasing mesh sizes, thus verifying the convergence of the numerical scheme presented herein.

For rather long calculation times, greater than five times the width of the pressure pulse, instability of the solutions started to show clearly at points on the axis of symmetry, especially those situated on the layers interfaces. In order to get around this difficulty, linear artificial viscosity terms are introduced into the equations of motion (4):

$$\begin{aligned} \frac{\partial}{\partial r}(\sigma_r + q_r) + \frac{\partial \tau_{rz}}{\partial z} + \frac{\sigma_r - \sigma_\theta}{r} &= \zeta \ddot{u}, \\ \frac{\partial \tau_{rz}}{\partial r} + \frac{\partial}{\partial z}(\sigma_z + q_z) + \frac{\tau_{rz}}{r} &= \zeta \ddot{w}, \end{aligned} \tag{57}$$

where

$$q_r = \zeta \Gamma c_d \Delta r \left(\frac{\partial \dot{u}}{\partial r}\right), \qquad q_z = \zeta \Gamma c_d \Delta z \left(\frac{\partial \dot{w}}{\partial z}\right), \tag{58}$$

in which Γ is a dimensionless viscosity coefficient. Values of Γ ranging from 0.2–0.6 proved to be suitable for the present investigation. As a consequence of (57), the accelerations $\ddot{u}_1$ and $\ddot{w}_1$ derived from (3), Fig. 1, must be modified as follows:

$$\ddot{u}_1^{t+\Delta t} = \ddot{u}_1'^{t-\Delta t} + \delta \ddot{u}_1, \qquad \ddot{w}_1^{t+\Delta t} = \ddot{w}_1'^{t+\Delta t} + \delta \ddot{w}_1, \tag{59}$$

where $\ddot{u}_1'$ and $\ddot{w}_1'$ are the unmodified accelerations, and

$$\begin{aligned} \delta \ddot{u}_1 &= \Gamma(\dot{u}_2{}^t - 2\dot{u}_1{}^t + \dot{u}_7{}^t)\, c_d/\Delta r, \\ \delta \ddot{w}_1 &= \Gamma(\dot{w}_8{}^t - 2\dot{w}_1{}^t + \dot{w}_6{}^t)\, c_d/\Delta z. \end{aligned} \tag{60}$$

It was observed that, the artificial viscosity terms q_r and q_z as introduced in (57) made the numerical scheme conditionally stable; see Appendix. The artificial viscosity terms, however, did not alter the significant features of the solutions.

6. Specific Problems

Numerical solutions for two specific problems are presented and discussed. Both problems are concerned with stress wave propagation in elastic-plastic layered half spaces subjected to applied pressures on the surface boundary as shown in Fig. 3.

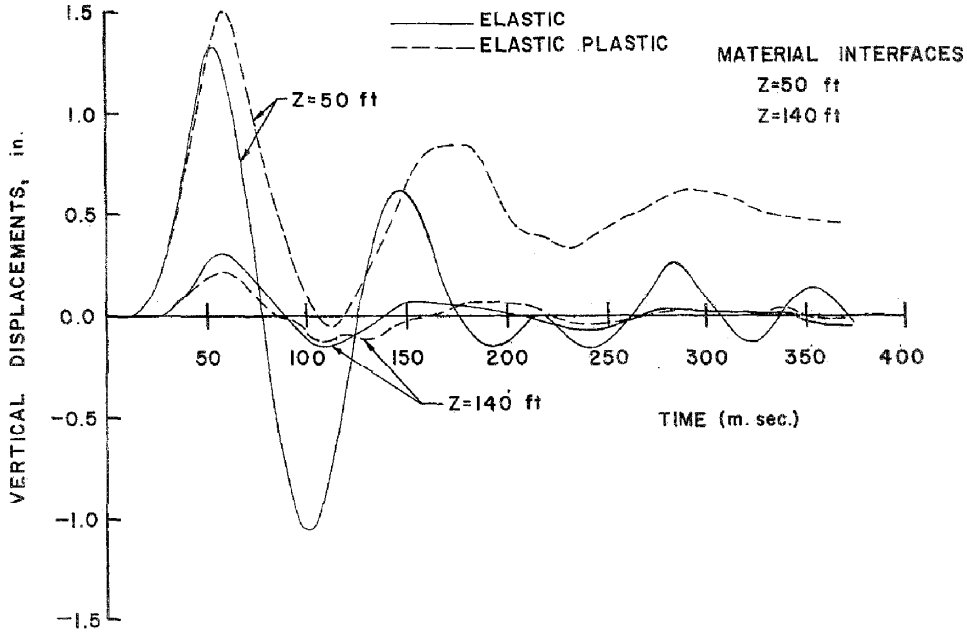

FIG. 12. History of vertical displacement at $R = 0$ ft.

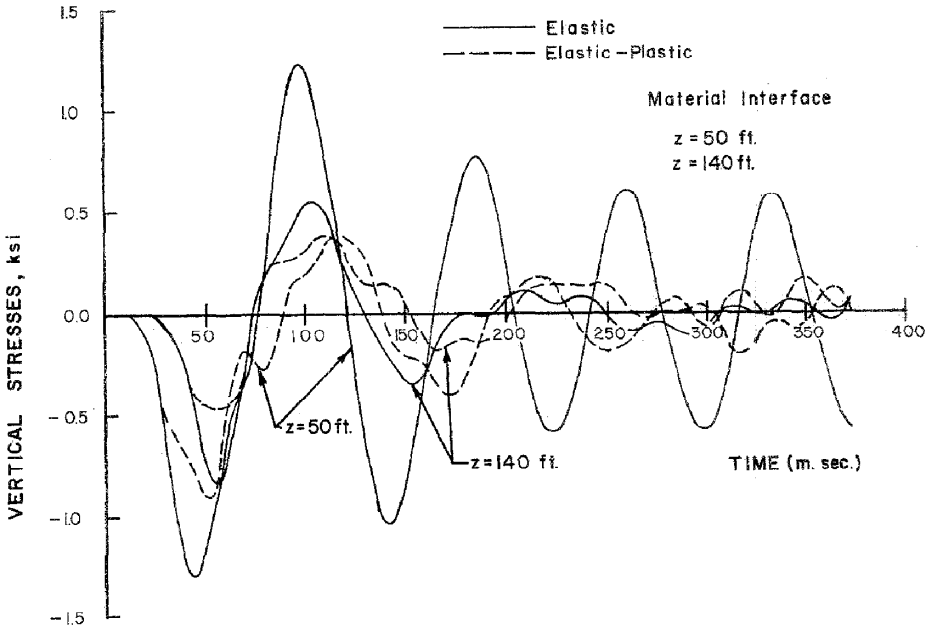

FIG. 13. History of vertical stresses at $R = 0$ ft.

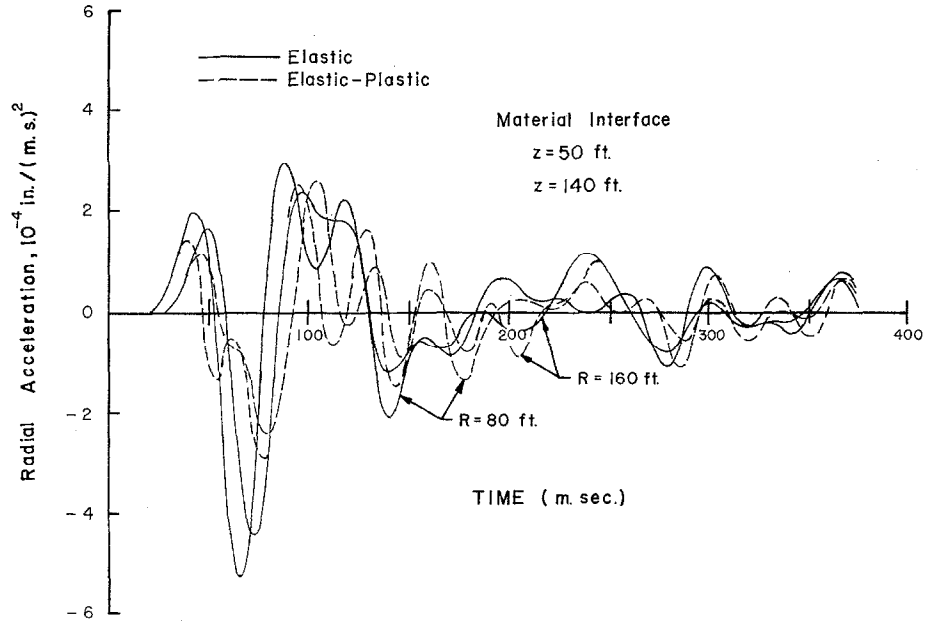

FIG. 14. History of radial accelerations at $Z = 140$ ft.

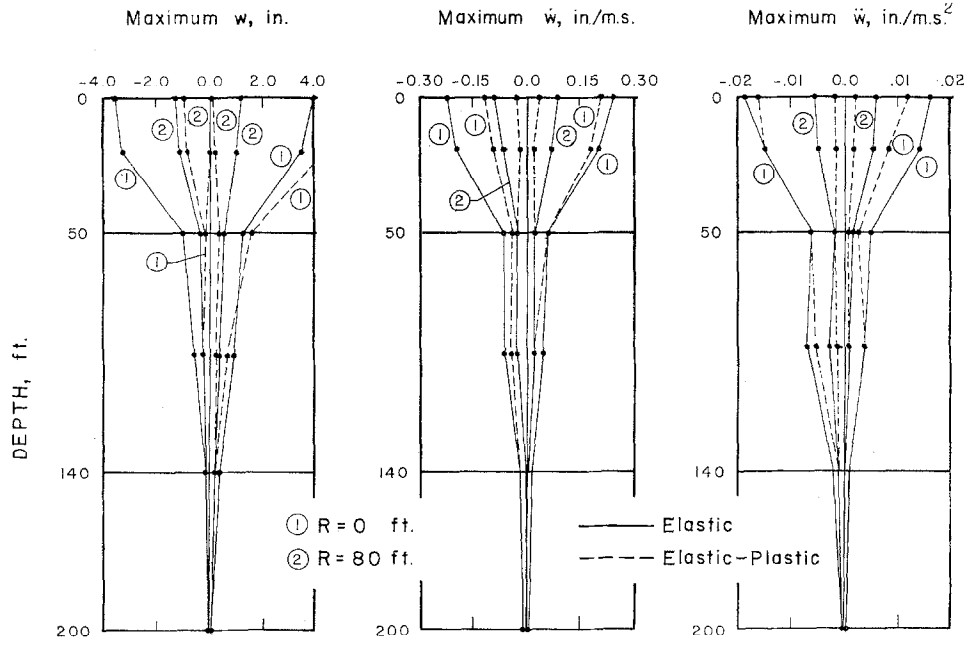

FIG. 15. Maximum vertical motions vs. depth.

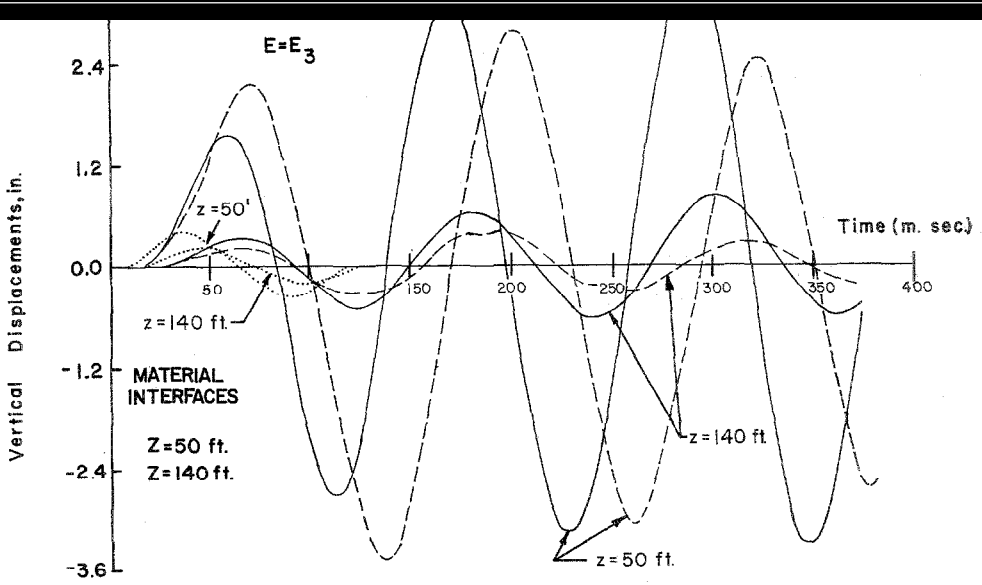

FIG. 16. History of vertical displacements at $R = 0$ ft (sinusoidal loading).

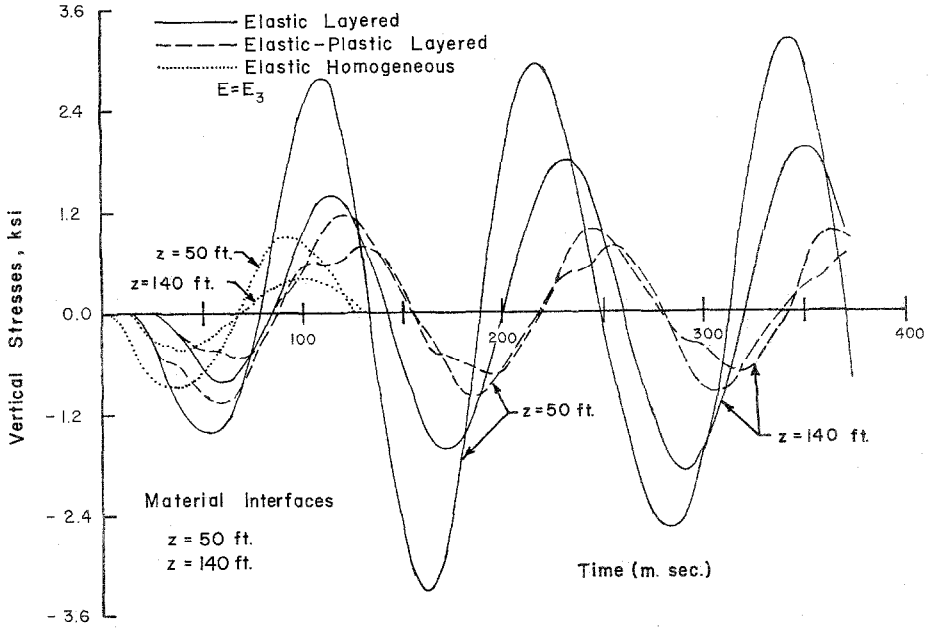

FIG. 17. History of vertical stresses at $R = 0$ ft (sinusoidal loading).

Wave Motion in a Layered Solid Medium Induced by a Blast Loading

The blast pressure pulse is shown in Fig. 8. The half space considered is like that in Fig. 3 (where the right edge is confined laterally), with $H_1 = 50$ ft, $H_2 = 90$ ft, and $R_b = 80$ ft. The material constants of the different layers are:

$$E_1 = 154 \text{ ksi}, \quad E_2 = 888 \text{ ksi}, \quad E_3 = 2465 \text{ ksi},$$

$$c_{d_1} = 2500 \text{ fps}, \quad c_{d_2} = 600 \text{ fps}, \quad c_{d_3} = 10000 \text{ fps},$$

$$\zeta = 140 \text{ lb/ft}^3, \quad \nu = 0.26, \quad k_{0_1} = 0.15 \text{ ksi}, \quad k_{0_2} = 0.30 \text{ ksi},$$

and the thid layer is assumed to remain elastic. The space and time meshes used are:

$$\Delta z_1 = 25 \text{ ft}, \quad \Delta z_2 = 30 \text{ ft}, \quad \Delta z_3 = 40 \text{ ft},$$

$$\Delta r = 40 \text{ ft}, \quad \Delta t = 0.75 \text{ msec}.$$

The results are summarized in Figs. 12 through 15. They generally indicate that plastic yielding of the softer top layer led to higher magnitudes of displacements and lower magnitudes of stresses than those of the corresponding elastic material, as should be expected. Figure 13 shows that the elastic vertical stresses at a point on the first material interface oscillate as a result of reflections from the surface and the second material interface. These ocillations occur also at the second interface; however, these latter oscillations are not as severe, since there are no reflections from the transmitting boundary. A space plot of the variation of the maximum vertical displacements, velocities, and accelerations with depth is shown in Fig. 15.

A Layered Half Space Subjected to Sinusoidal Loading

A continuously applied sinusoidal pressure pulse of amplitude 1.0 ksi and period 120 msec is assumed to be acting on the above layered half space with the same space and time mesh sizes. Assuming that tensile loading is admissible, Figs. 16 and 17 show the history of vertical displacements and stresses.

7. Conclusions

The mathematical analysis of wave motion in layered elastic-plastic half spaces is a difficult problem. A discrete-variable approach proves to be feasible. The lumped parameter model described herein provides a powerful tool for formulating a numerical solution, which is highly adaptable to electronic computations, from the simple principles of mechanics.

The resulting numerical scheme is essentially unstable for the axisymmetric case, because of local instabilities in the neighborhood of the axis of symmetry. Such instability starts to show in the numerical solution only after long calculation times (5–6 times the width of the pressure pulse).

APPENDIX. Effect of Artificial Viscosity on Stability of the Difference Scheme

It was observed earlier that in view of the results shown in Fig. 7, the differencing scheme is unstable for axisymmetric calculations. It will be shown that the same scheme becomes conditionally stable if artificial viscosity terms are added as in (57).

From (14) and (44), the velocities $\dot{u}^t$ and $\dot{w}^t$ are expressed as follows:

$$\dot{u}^t = (u^{t+\Delta t} - u^{t-\Delta t})/2\Delta t, \qquad \text{and} \qquad \dot{w}^t = (w^{t+\Delta t} - w^{t-\Delta t})/2\Delta t. \tag{61}$$

Consequently, the additional term to be added to the right side of (43) is

$$\frac{\partial q_r}{\partial r} = \zeta \Gamma c_d[\{u(i+2, j, k+1) - 2u(i, j, k+1) + u(i-2, j, k+1)] - [u(i+2, j, k-1) - 2u(i, j, k-1) + u(i-2, j, k-1)\}]/2\Delta t\, \Delta r. \tag{62}$$

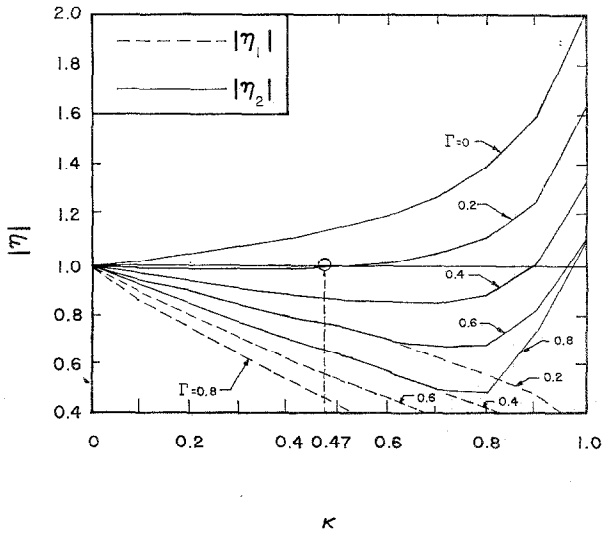

FIG. 18. Modulus of η vs. κ for $p = 1.0$, $\sin \beta\Delta z/2 = 1.0$.

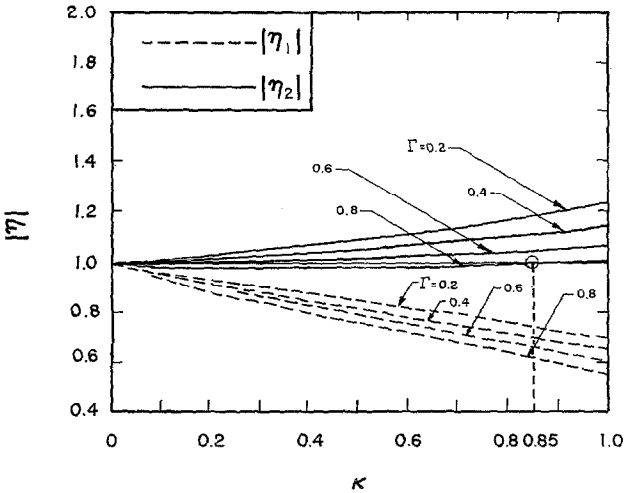

FIG. 19. Modulus of η vs. κ for $p = 1.0$, $\sin \beta \Delta z/2 = 0.5$.

Therefore, (47) is modified by the following additional term appearing on the right-hand side

$$2(\eta^{-1} - \eta) \cdot \zeta \Gamma c_a \sin^2(\alpha \Delta r/2)/\Delta t \Delta r. \tag{63}$$

Similarly, the right-hand side of (48) is modified by the term

$$2(\eta^{-1} - \eta) \cdot \zeta \Gamma c_a \sin^2(\beta \Delta z/2)/\Delta t \Delta z. \tag{64}$$

The resulting equations, derived from (47) and (48) by the addition of the above terms (63) and (64), can then be written as follows:

$$A_1\eta^2 - 2\eta B_1 + C_1 = 0, \tag{65}$$

$$A_2\eta^2 - 2\eta B_2 + C_2 = 0, \tag{66}$$

respectively, where A_1, A_2,..., are coefficients that can be derived through lengthy substitutions. Choosing, $p = 1.0$ and $\Delta r = \Delta z$ which happened to give larger values of $|\eta|$, Fig. 7, and, without any loss of generality, taking the frequencies α and β to be equal, the coefficients in (65) and (66) can be greatly simplified. Once more it can be easily found that $|B_2| > |B_1|$; hence the maximum modulus of η is obtained from (66) which can be expressed as

$$\eta^2 - 2\eta B + C = 0, \tag{67}$$

where

$$B = \frac{1 - 2\kappa^2 \sin^2\theta}{1 + \sqrt{2}\Gamma\kappa \sin^2\theta} + I\frac{(\kappa^2 \sin\theta)/2}{1 + \sqrt{2}\Gamma\kappa \sin^2\theta}, \tag{68}$$

$$C = \frac{1 - \sqrt{2}\Gamma\kappa \sin^2\theta}{1 + \sqrt{2}\Gamma\kappa \sin^2\theta}, \tag{69}$$

in which κ and Γ are as defined before, and $\theta = \alpha\Delta r/2 = \beta\Delta z/2$.

For $\sin\theta = 0$, it is clear that $|\eta| = 1$; hence the absolute values of the roots of (67) are evaluated numerically for $\sin\theta = 0.5$ and 1.0 respectively. The results are shown in Figs. 18 and 19. They show clearly that, by using artificial viscosity, the numerical scheme can be made conditionally stable. Since the purpose of artificial viscosity is to insure stability of the scheme without sacrificing the accuracy of the results, then, whenever possible, a smaller value of Γ should be used in the calculations. It may also be observed that the stability criterion used in this study $\Delta t \leqslant \Delta z/3c_d$, which is equivalent to $\kappa \leqslant 0.47$, proved to be quite adequate with artificial viscosity coefficients Γ varying from 0.20 to 0.60.

ACKOWLEDGMENT

This paper is extracted from a Ph.D. thesis in Civil Engineering at the University of Illinois [13]. The author wishes to thank Professor A. Ang for his valuable suggestions as thesis advisor. The study was supported in part by the National Science Foundation through Research Grant No. GK589.

REFERENCES

1. L. M. BREKHOVSKIKH, "Waves in Layered Media," (translated from Russian) Academic Press, New York 1960.
2. W. M. EWING, W. S. JARDETZKY, AND F. PRESS, "Elastic Waves in Layered Media," International Series in the Earth Sciences, McGraw-Hill, New York, 1957.
3. K. KOLSKY, "Stress Waves in Solids," Dover, New York 1963.
4. W. OLSZAK, Z. MROZ AND P. PERZYNA, "Recent Trends in the Development of the Theory of Plasticity," A Pergamon Press Book, Macmillan Co., New York, 1963.
5. C. L. PEKERIS ET AL., Propagation of a compressional pulse in a layered solid, *Rev. Geophys.* **3** (1965), 25–47.
6. Z. ALTERMAN AND F. C. KARAL, Propagation of elastic waves in layered media by finite difference methods, *Bull. Seismological Soc. Amer.* **58** (1968), 367–398.
7. G. MAENCHEN AND S. SACK, The tensor code, *in* "Methods in Computational Physics," Vol. 3, pp. 181–210, Academic Press, 1964.
8. M. L. WILKINS, "Calculation of elastic-plastic flow," *in* "Methods in Computational Physics," Vol. 3, pp. 211–263 Academic Press, 1964.

9. A. H.-S. ANG AND J. H. RAINER, "A Model for wave motions in Axisymmetric solids," *J. Eng. Mech. Div.* American Society of Civil Engineers **90** (1964), EM2, 195–223.
10. R. HILL, "The Mathematical Theory of Plasticity," Oxford University Press, London/ New York, 1950.
11. W. PRAGER AND P. G. HODGE, "Theory of Perfectly Plastic Solids," John Wiley and Sons, New York, 1961.
12. S. TIMOSHENKO AND J. N. GOODIER, "Theory of Elasticity," McGraw–Hill, New York, 1951.
13. A. H. SAMEH, "Numerical analysis of axisymmetric wave propagation in elastic-plastic layered media," Ph.D. Thesis, Department of Civil Engineering, University of Illinois, Urbana, Ill., 1968.
14. R. COURANT, K. FRIEDRICHS AND H. LEWY, On the partial difference equations of mathematical physics, *IBM J.*, 215–234 (March 1967).
15. G. E. FORSYTHE AND R. W. WASOW, "Finite-Difference Methods for Partial Differential Equations," John Wiley and Sons, New York, 1960.
16. L. FOX, "Numerical Solution of Ordinary and Partial Differential Equations," Addison–Wesley, Reading, Mass., 1962.
17. S. K. GODUNOV AND V. S. RYABENKI, "Theory of Difference Schemes" (translated from Russian), North–Holland, Amsterdam, 1964.
18. R. D. RICHTMYER AND K. W. MORTON, "Difference Methods for Initial-Value Problems," 2nd ed., Interscience, New York, 1967.
19. J. VON NEUMANN AND R. D. RICHTMYER, A method for the numerical calculation of hydrodynamic shocks, *J. Appl. Phys.* **21** (1950), 232–237.
20. G. G. O'BRIEN, M. A. HYMAN, AND S. KAPLAN, A study of the numerical solution of partial differential equations, *J. Math. Phys.* **29** (1951), 223–251.